Original Article

Institution of MECHANICAL ENGINEERS
Journal of AEROSPACE ENGINEERING

Proc IMechE Part G:
J Aerospace Engineering
2014, Vol. 228(6) 960–979

DOI: 10.1177/0954410013485697
uk.sagepub.com/jaero
SAGE

An assessment of thrust vector concepts for twin-engine airplane

AK Vinayagam and Nandan K Sinha

Abstract

Thrust vector nozzles are finding place on modern fighter airplanes because of the benefits they provide and also due to diminishing weight penalty of such nozzles. They offer additional benefits in the case of a twin-engine airplane. Different vectoring configurations such as multi-axis vectoring, single-axis pitch vectoring and single-axis vectoring with canted nozzles have been studied with respect to twin-engine airplane configuration. Modeling and integration of thrust vector nozzles with rigid airplane six-degrees-of-freedom equations of motion have been carried out in this article. Using the integrated model, a comparative study is carried out to summarize the capabilities and limitations of various nozzle configurations with respect to performance of an airplane in velocity vector roll and in Herbst maneuvers. The airplane model used in this work is the F-18/HARV and all simulation results have been produced using a nonlinear dynamic inversion controller developed in Matlab/Simulink environment. Results show that a multi-axis thrust vectoring provides additional benefits as compared to single-axis vectoring with canted nozzles in high angle of attack velocity vector roll and in Herbst maneuvers. The single-axis pitch only vectoring has roll control power and lacks in yaw control power, to execute the velocity vector roll maneuver.

Keywords

Vector nozzle, thrust vector control, nonlinear dynamic inversion controller, velocity vector roll, Herbst maneuver, heading angle, gross thrust, high AOA, canted nozzles

Date received: 15 September 2012; accepted: 13 March 2013

Introduction

Thrust vector nozzles are increasingly finding place on modern fighter airplanes. This is due to the benefits they provide in enhancing the agility of the airplane on the one hand and decreasing weight penalty of the vector nozzle hardware on the other hand. Vector nozzles have been tested on many experimental airplanes such as F-18/HARV, X-31, F-15 ACTIVE and F-16 VISTA and they have been flying on Su-30 MKI, F-22, JSF and MIG-29 OVT. F-18/HARV and X-31 airplanes use airframe mounted post-exit vanes to deflect the jet. F-22 uses two-dimensional (2-D) nozzle, which can deflect only about the pitch axis, whereas F-15 ACTIVE and F-16 VISTA use multi-axis vector nozzles and Su-30 MKI uses single-axis vectoring with canted nozzles. The canted nozzles vector in a plane inclined at an angle to the symmetry plane and the left and the right nozzles are canted in opposite directions. An assessment of these concepts from maneuverability point of view using velocity vector roll (VVR) as the base maneuver is the objective of this study.

VVR is an air combat maneuver. It is a highly dynamic maneuver with strong inertia coupling. The VVR rate achievable by an airplane is drastically reduced as the airplane speed decreases. Especially at high angles of attack, the VVR demands large control power from elevator, aileron and rudder together due to inertia coupling. As the available aerodynamic control power is small at low speeds and high angles of attack, airplanes virtually cannot carry out VVR using the aerodynamic controls alone. The thrust vector nozzle can play a crucial role in this part of the flight envelope.

Although there are published literature works with regard to the multi-axis vector nozzle simulation studies, there is not much information available in open literature on the pitch only vector nozzle and single-axis vectoring with canted nozzles. This study is motivated toward understanding the comparative

Department of Aerospace Engineering, Indian Institute of Technology Madras, Chennai, India

Corresponding author:
AK Vinayagam, Department of Aerospace Engineering, Indian Institute of Technology Madras, Chennai-600036, India.
Email: vinayagam@jetmail.ada.gov.in

effectiveness of the thrust vector nozzle concepts. Capone and Mason[1] conducted experiments on single-axis canted 2-D nozzles to evaluate the pitch and yaw control power. O'Rourke et al.[2] carried out a PC-based simulation on F-16 MATV with VVR at 35° angle of attack (AOA). The YF-22 prototype[3] demonstrated VVR up to 60° AOA. It used the pitch only thrust vector nozzles to control the pitch divergence. Blending of aerodynamic and thrust vector control (TVC) for VVR control was discussed by Atesoglu and Ozgoren.[4] Inertial and aerodynamic coupling between longitudinal and lateral/directional dynamics was discussed in ref. [5] It has been pointed out in ref. [5] that thrust vectoring can provide sufficient stability and control augmentation above 40° AOA in the yaw axis to compensate for rudder effectiveness. Sinha and Ananthkrishnan[6] and Goman et al.[7] have used reduced order models to analyze VVR maneuver and computed pseudo-steady-state roll rate with aerodynamic controls only. The control allocation techniques in the presence of TVC were studied by Scalera[8] and Bundick et al.[9]

In this work, the thrust vector model equations have been derived first and a critical analysis of the control authority of each thrust vector concept is carried out. A six-degrees-of-freedom (dof) simulation model of F-18/HARV with nonlinear dynamic inversion (NDI) controller has been developed in Matlab incorporating the thrust vector nozzles. A comparative analysis of thrust vector concepts is carried out through simulation studies of airplane in VVR and Herbst maneuvers.

Thrust vector models

A simple thrust vector model was used for the analysis in this work as shown in Figure 1.

Sign conventions

The downward nozzle deflection is considered to be positive, similar to elevator and both of them produce negative pitching moment (nose down) for the positive deflection. The leftward nozzle deflection is considered to be positive, similar to rudder and both produce negative yawing moment (yaw left). In the case of asymmetric deflection of the twin-engine airplane nozzles, the right nozzle deflection downward and the left nozzle upward are considered to be positive. This results in a negative rolling moment (roll to the left) for positive deflection similar to ailerons.

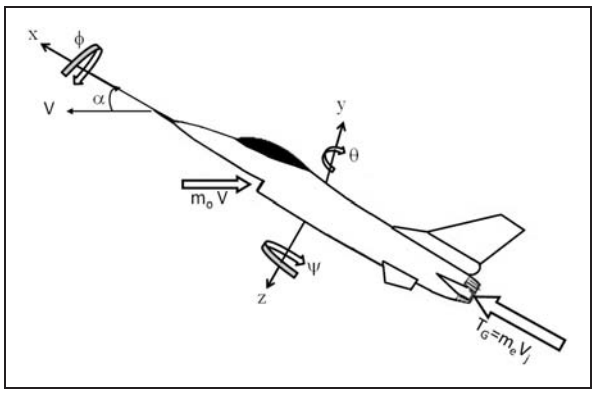

Figure 1. Propulsion system forces.

Thrust vector forces and moments

The gross thrust deflected by δ_{ptv} and δ_{ytv} in the pitch and yaw directions, respectively, are resolved into the body-axis components. Similarly, the inlet drag is also resolved into body-axis components. The resulting forces are

$$\left.\begin{aligned} T_{Gx} &= T_G \cos\,\delta_{ptv} \cos\,\delta_{ytv} S \\ T_{Gy} &= T_G \cos\,\delta_{ptv} \sin\,\delta_{ytv} S \\ T_{Gz} &= -T_G \sin\,\delta_{ptv} \cos\,\delta_{ytv} S \end{aligned}\right\} \quad (1)$$

where

$$S = \frac{1}{\sqrt{\cos^2\delta_{ptv} + \cos^2\delta_{ytv}\sin^2\delta_{ptv}}}$$

Force components on the air inlet

$$\left.\begin{aligned} T_{INx} &= -m_0 V \cos\alpha\cos\beta \\ T_{INy} &= -m_0 V \sin\,\beta \\ T_{INz} &= -m_0 V \sin\alpha\cos\beta \end{aligned}\right\} \quad (2)$$

At low speeds, forces on the inlet are small. Total thrust forces are thus written as

$$\left.\begin{aligned} T_x &= T_{Gx} + T_{INx} \\ T_y &= T_{Gy} + T_{INy} \\ T_z &= T_{Gz} + T_{INz} \end{aligned}\right\} \quad (3)$$

The total moments due to thrust forces are

$$\left.\begin{aligned} M_x &= -T_{Gy}(Z_{eng} - Z_{CG}) + T_{Gz}(Y_{eng} - Y_{CG}) \\ &\quad -T_{INy}(Z_{inlet} - Z_{CG}) + T_{INz}(Y_{inlet} - Y_{CG}) \\ M_y &= T_{Gx}(Z_{eng} - Z_{CG}) + T_{Gz}(X_{CG} - X_{noz}) \\ &\quad +T_{Gx}(Z_{inlet} - Z_{CG}) + T_{Gz}(X_{CG} - X_{inlet}) \\ M_z &= -T_{Gx}(Y_{eng} - Y_{CG}) - T_{Gy}(X_{CG} - X_{noz}) \\ &\quad -T_{INx}(Y_{inlet} - Y_{CG}) - T_{INy}(X_{CG} - X_{inlet}) \end{aligned}\right\} \quad (4)$$

Forces and moments due to thrust vectoring for different cases are discussed below. For simplicity, forces on the air inlet are ignored in the

subsequent discussions. These forces are small at low speeds where the TVC is generally used.

Single-axis pitch only vectoring

For *symmetric deflection of the nozzles* (twin-engine airplane), neglecting the forces on the air inlet, forces and moments can be summarized as

$$\left.\begin{aligned} T_x &= 2T_G \cos\,\delta_{ptv} \\ T_y &= 0 \\ T_z &= -2T_G \sin\,\delta_{ptv} \end{aligned}\right\} \tag{5}$$

$$\left.\begin{aligned} M_x &= 0 \\ M_y &= 2T_G \cos\,\delta_{ptv}(Z_{eng} - Z_{CG}) \\ &\quad -2T_G \sin\,\delta_{ptv}(X_{CG} - X_{noz}) \\ M_z &= 0 \end{aligned}\right\} \tag{6}$$

and for *anti-symmetric deflection of the nozzles*

$$\left.\begin{aligned} T_x &= 2T_G \cos\,\delta_{ptv} \\ T_y &= 0 \\ T_z &= 0 \end{aligned}\right\} \tag{7}$$

$$\left.\begin{aligned} M_x &= 2T_G \sin\,\delta_{ptv} Y_{eng} \\ M_y &= 2T_G \cos\,\delta_{ptv}(Z_{eng} - Z_{CG}) \\ M_z &= 0 \end{aligned}\right\} \tag{8}$$

In the case of symmetric deflection, pure pitching moment is produced as the rolling moment created by left and right nozzles cancel each other. In the case of anti-symmetric deflection, the net pitching moment is zero, but the opposite z-component forces produce a rolling moment. The vertical offset of center of gravity (CG) from engine axis is usually small.

Single-axis vectoring with canted nozzles

A schematic diagram of single-axis vectoring with canted nozzles is shown in Figure 2. Symmetric and anti-symmetric deflections of left/right nozzles on a twin-engine airplane are shown in Figure 2(a) and (b), respectively. The plane of vectoring is inclined at an angle ϕ_N to the vertical plane, i.e. the nozzles are canted by an angle ϕ_N. Left and right nozzle vectoring planes are inclined in opposite directions such that the equal symmetric deflections cancel the side

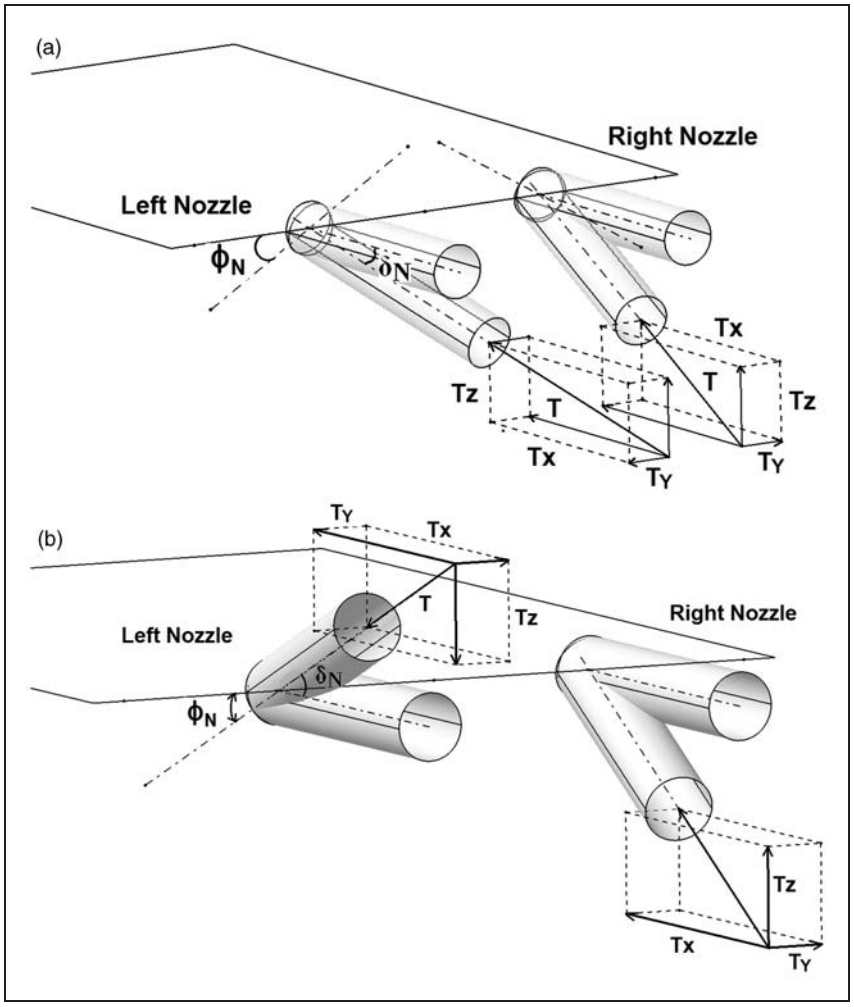

Figure 2. (a) Symmetric deflection of the canted nozzles and (b) anti-symmetric deflection of the canted nozzles.

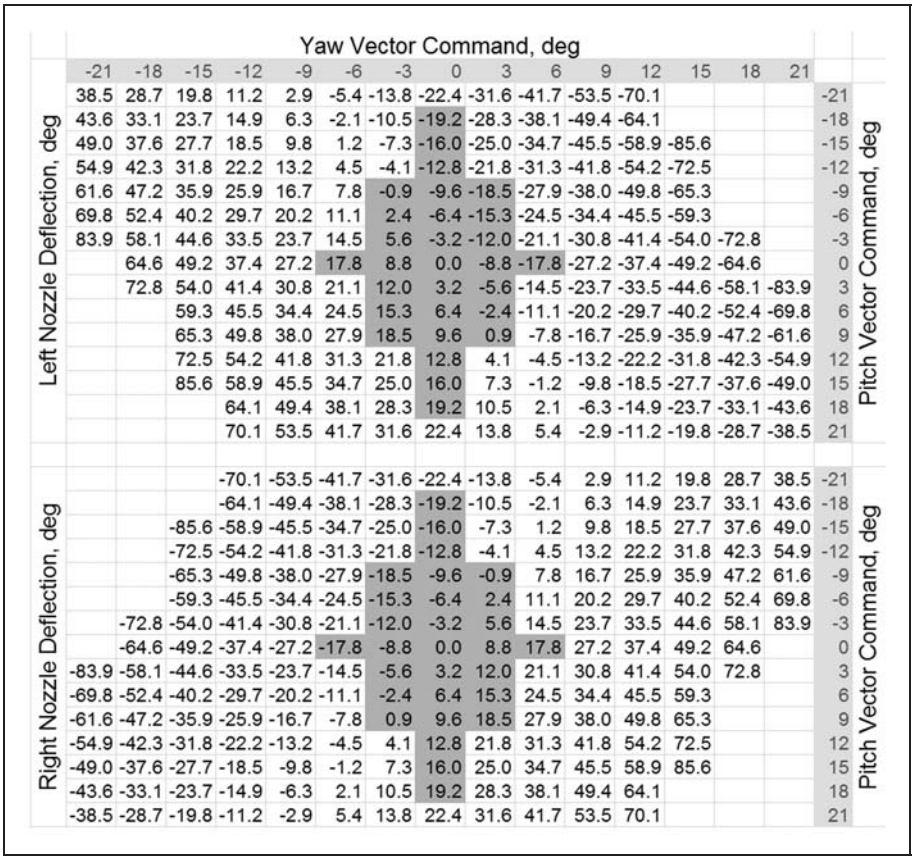

Left Nozzle Deflection, deg \ Yaw Vector Command, deg	-21	-18	-15	-12	-9	-6	-3	0	3	6	9	12	15	18	21	Pitch Vector Command, deg
	38.5	28.7	19.8	11.2	2.9	-5.4	-13.8	-22.4	-31.6	-41.7	-53.5	-70.1				-21
	43.6	33.1	23.7	14.9	6.3	-2.1	-10.5	-19.2	-28.3	-38.1	-49.4	-64.1				-18
	49.0	37.6	27.7	18.5	9.8	1.2	-7.3	-16.0	-25.0	-34.7	-45.5	-58.9	-85.6			-15
	54.9	42.3	31.8	22.2	13.2	4.5	-4.1	-12.8	-21.8	-31.3	-41.8	-54.2	-72.5			-12
	61.6	47.2	35.9	25.9	16.7	7.8	-0.9	-9.6	-18.5	-27.9	-38.0	-49.8	-65.3			-9
	69.8	52.4	40.2	29.7	20.2	11.1	2.4	-6.4	-15.3	-24.5	-34.4	-45.5	-59.3			-6
	83.9	58.1	44.6	33.5	23.7	14.5	5.6	-3.2	-12.0	-21.1	-30.8	-41.4	-54.0	-72.8		-3
		64.6	49.2	37.4	27.2	17.8	8.8	0.0	-8.8	-17.8	-27.2	-37.4	-49.2	-64.6		0
		72.8	54.0	41.4	30.8	21.1	12.0	3.2	-5.6	-14.5	-23.7	-33.5	-44.6	-58.1	-83.9	3
			59.3	45.5	34.4	24.5	15.3	6.4	-2.4	-11.1	-20.2	-29.7	-40.2	-52.4	-69.8	6
			65.3	49.8	38.0	27.9	18.5	9.6	0.9	-7.8	-16.7	-25.9	-35.9	-47.2	-61.6	9
			72.5	54.2	41.8	31.3	21.8	12.8	4.1	-4.5	-13.2	-22.2	-31.8	-42.3	-54.9	12
			85.6	58.9	45.5	34.7	25.0	16.0	7.3	-1.2	-9.8	-18.5	-27.7	-37.6	-49.0	15
				64.1	49.4	38.1	28.3	19.2	10.5	2.1	-6.3	-14.9	-23.7	-33.1	-43.6	18
				70.1	53.5	41.7	31.6	22.4	13.8	5.4	-2.9	-11.2	-19.8	-28.7	-38.5	21

Right Nozzle Deflection, deg \ Yaw Vector Command, deg	-21	-18	-15	-12	-9	-6	-3	0	3	6	9	12	15	18	21	Pitch Vector Command, deg
				-70.1	-53.5	-41.7	-31.6	-22.4	-13.8	-5.4	2.9	11.2	19.8	28.7	38.5	-21
				-64.1	-49.4	-38.1	-28.3	-19.2	-10.5	-2.1	6.3	14.9	23.7	33.1	43.6	-18
			-85.6	-58.9	-45.5	-34.7	-25.0	-16.0	-7.3	1.2	9.8	18.5	27.7	37.6	49.0	-15
			-72.5	-54.2	-41.8	-31.3	-21.8	-12.8	-4.1	4.5	13.2	22.2	31.8	42.3	54.9	-12
			-65.3	-49.8	-38.0	-27.9	-18.5	-9.6	-0.9	7.8	16.7	25.9	35.9	47.2	61.6	-9
			-59.3	-45.5	-34.4	-24.5	-15.3	-6.4	2.4	11.1	20.2	29.7	40.2	52.4	69.8	-6
		-72.8	-54.0	-41.4	-30.8	-21.1	-12.0	-3.2	5.6	14.5	23.7	33.5	44.6	58.1	83.9	-3
		-64.6	-49.2	-37.4	-27.2	-17.8	-8.8	0.0	8.8	17.8	27.2	37.4	49.2	64.6		0
-83.9	-58.1	-44.6	-33.5	-23.7	-14.5	-5.6	3.2	12.0	21.1	30.8	41.4	54.0	72.8			3
-69.8	-52.4	-40.2	-29.7	-20.2	-11.1	-2.4	6.4	15.3	24.5	34.4	45.5	59.3				6
-61.6	-47.2	-35.9	-25.9	-16.7	-7.8	0.9	9.6	18.5	27.9	38.0	49.8	65.3				9
-54.9	-42.3	-31.8	-22.2	-13.2	-4.5	4.1	12.8	21.8	31.3	41.8	54.2	72.5				12
-49.0	-37.6	-27.7	-18.5	-9.8	-1.2	7.3	16.0	25.0	34.7	45.5	58.9	85.6				15
-43.6	-33.1	-23.7	-14.9	-6.3	2.1	10.5	19.2	28.3	38.1	49.4	64.1					18
-38.5	-28.7	-19.8	-11.2	-2.9	5.4	13.8	22.4	31.6	41.7	53.5	70.1					21

Figure 3. Control authority: nozzle cant angle 20°.

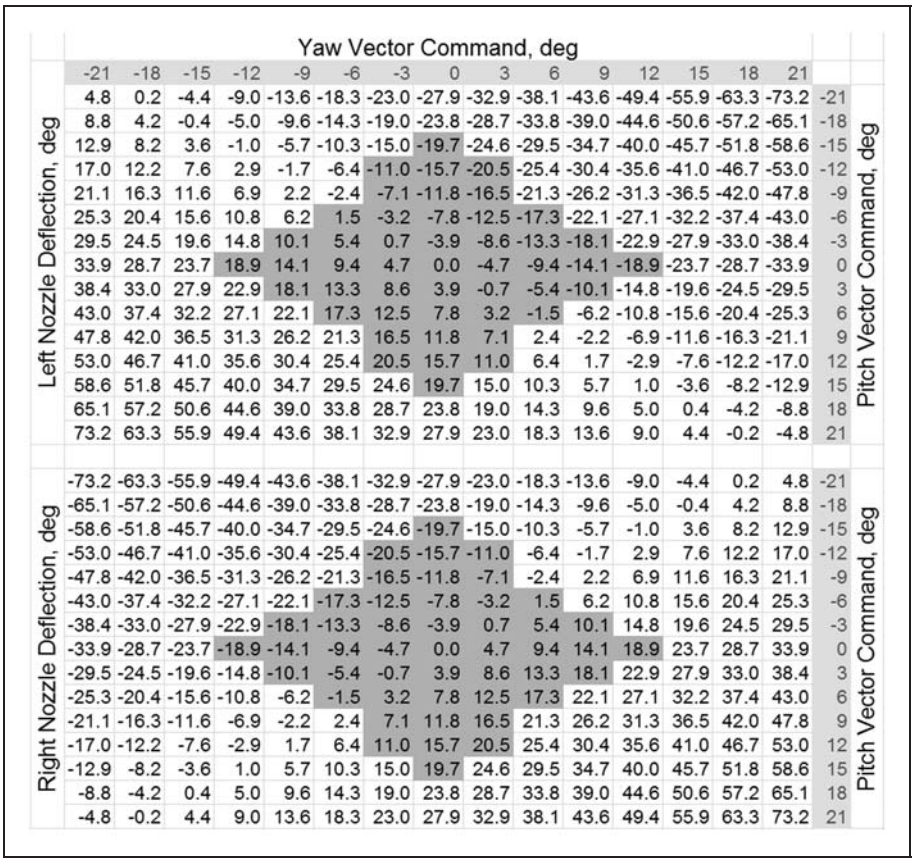

Left Nozzle Deflection, deg \ Yaw Vector Command, deg	-21	-18	-15	-12	-9	-6	-3	0	3	6	9	12	15	18	21	Pitch Vector Command, deg
	4.8	0.2	-4.4	-9.0	-13.6	-18.3	-23.0	-27.9	-32.9	-38.1	-43.6	-49.4	-55.9	-63.3	-73.2	-21
	8.8	4.2	-0.4	-5.0	-9.6	-14.3	-19.0	-23.8	-28.7	-33.8	-39.0	-44.6	-50.6	-57.2	-65.1	-18
	12.9	8.2	3.6	-1.0	-5.7	-10.3	-15.0	-19.7	-24.6	-29.5	-34.7	-40.0	-45.7	-51.8	-58.6	-15
	17.0	12.2	7.6	2.9	-1.7	-6.4	-11.0	-15.7	-20.5	-25.4	-30.4	-35.6	-41.0	-46.7	-53.0	-12
	21.1	16.3	11.6	6.9	2.2	-2.4	-7.1	-11.8	-16.5	-21.3	-26.2	-31.3	-36.5	-42.0	-47.8	-9
	25.3	20.4	15.6	10.8	6.2	1.5	-3.2	-7.8	-12.5	-17.3	-22.1	-27.1	-32.2	-37.4	-43.0	-6
	29.5	24.5	19.6	14.8	10.1	5.4	0.7	-3.9	-8.6	-13.3	-18.1	-22.9	-27.9	-33.0	-38.4	-3
	33.9	28.7	23.7	18.9	14.1	9.4	4.7	0.0	-4.7	-9.4	-14.1	-18.9	-23.7	-28.7	-33.9	0
	38.4	33.0	27.9	22.9	18.1	13.3	8.6	3.9	-0.7	-5.4	-10.1	-14.8	-19.6	-24.5	-29.5	3
	43.0	37.4	32.2	27.1	22.1	17.3	12.5	7.8	3.2	-1.5	-6.2	-10.8	-15.6	-20.4	-25.3	6
	47.8	42.0	36.5	31.3	26.2	21.3	16.5	11.8	7.1	2.4	-2.2	-6.9	-11.6	-16.3	-21.1	9
	53.0	46.7	41.0	35.6	30.4	25.4	20.5	15.7	11.0	6.4	1.7	-2.9	-7.6	-12.2	-17.0	12
	58.6	51.8	45.7	40.0	34.7	29.5	24.6	19.7	15.0	10.3	5.7	1.0	-3.6	-8.2	-12.9	15
	65.1	57.2	50.6	44.6	39.0	33.8	28.7	23.8	19.0	14.3	9.6	5.0	0.4	-4.2	-8.8	18
	73.2	63.3	55.9	49.4	43.6	38.1	32.9	27.9	23.0	18.3	13.6	9.0	4.4	-0.2	-4.8	21

Right Nozzle Deflection, deg \ Yaw Vector Command, deg	-21	-18	-15	-12	-9	-6	-3	0	3	6	9	12	15	18	21	Pitch Vector Command, deg
-73.2	-63.3	-55.9	-49.4	-43.6	-38.1	-32.9	-27.9	-23.0	-18.3	-13.6	-9.0	-4.4	0.2	4.8		-21
-65.1	-57.2	-50.6	-44.6	-39.0	-33.8	-28.7	-23.8	-19.0	-14.3	-9.6	-5.0	-0.4	4.2	8.8		-18
-58.6	-51.8	-45.7	-40.0	-34.7	-29.5	-24.6	-19.7	-15.0	-10.3	-5.7	-1.0	3.6	8.2	12.9		-15
-53.0	-46.7	-41.0	-35.6	-30.4	-25.4	-20.5	-15.7	-11.0	-6.4	-1.7	2.9	7.6	12.2	17.0		-12
-47.8	-42.0	-36.5	-31.3	-26.2	-21.3	-16.5	-11.8	-7.1	-2.4	2.2	6.9	11.6	16.3	21.1		-9
-43.0	-37.4	-32.2	-27.1	-22.1	-17.3	-12.5	-7.8	-3.2	1.5	6.2	10.8	15.6	20.4	25.3		-6
-38.4	-33.0	-27.9	-22.9	-18.1	-13.3	-8.6	-3.9	0.7	5.4	10.1	14.8	19.6	24.5	29.5		-3
-33.9	-28.7	-23.7	-18.9	-14.1	-9.4	-4.7	0.0	4.7	9.4	14.1	18.9	23.7	28.7	33.9		0
-29.5	-24.5	-19.6	-14.8	-10.1	-5.4	-0.7	3.9	8.6	13.3	18.1	22.9	27.9	33.0	38.4		3
-25.3	-20.4	-15.6	-10.8	-6.2	-1.5	3.2	7.8	12.5	17.3	22.1	27.1	32.2	37.4	43.0		6
-21.1	-16.3	-11.6	-6.9	-2.2	2.4	7.1	11.8	16.5	21.3	26.2	31.3	36.5	42.0	47.8		9
-17.0	-12.2	-7.6	-2.9	1.7	6.4	11.0	15.7	20.5	25.4	30.4	35.6	41.0	46.7	53.0		12
-12.9	-8.2	-3.6	1.0	5.7	10.3	15.0	19.7	24.6	29.5	34.7	40.0	45.7	51.8	58.6		15
-8.8	-4.2	0.4	5.0	9.6	14.3	19.0	23.8	28.7	33.8	39.0	44.6	50.6	57.2	65.1		18
-4.8	-0.2	4.4	9.0	13.6	18.3	23.0	27.9	32.9	38.1	43.6	49.4	55.9	63.3	73.2		21

Figure 4. Control authority: nozzle cant angle 40°.

Rolling Moment, kN-m/kN	Yaw Vector Command, deg															Pitch Vector Command, deg
	-21	-18	-15	-12	-9	-6	-3	0	3	6	9	12	15	18	21	
	0.80	0.69	0.58	0.46	0.35	0.23	0.12	0.00	-0.12	-0.23	-0.35	-0.46	-0.58	-0.69	-0.80	-21
	0.81	0.70	0.59	0.47	0.35	0.24	0.12	0.00	-0.12	-0.24	-0.35	-0.47	-0.59	-0.70	-0.81	-18
	0.83	0.71	0.60	0.48	0.36	0.24	0.12	0.00	-0.12	-0.24	-0.36	-0.48	-0.60	-0.71	-0.83	-15
	0.84	0.72	0.60	0.48	0.36	0.24	0.12	0.00	-0.12	-0.24	-0.36	-0.48	-0.60	-0.72	-0.84	-12
	0.84	0.73	0.61	0.49	0.37	0.25	0.12	0.00	-0.12	-0.25	-0.37	-0.49	-0.61	-0.73	-0.84	-9
	0.85	0.73	0.61	0.49	0.37	0.25	0.12	0.00	-0.12	-0.25	-0.37	-0.49	-0.61	-0.73	-0.85	-6
	0.85	0.74	0.62	0.49	0.37	0.25	0.12	0.00	-0.12	-0.25	-0.37	-0.49	-0.62	-0.74	-0.85	-3
	0.85	0.74	0.62	0.50	0.37	0.25	0.12	0.00	-0.12	-0.25	-0.37	-0.50	-0.62	-0.74	-0.85	0
	0.85	0.74	0.62	0.49	0.37	0.25	0.12	0.00	-0.12	-0.25	-0.37	-0.49	-0.62	-0.74	-0.85	3
	0.85	0.73	0.61	0.49	0.37	0.25	0.12	0.00	-0.12	-0.25	-0.37	-0.49	-0.61	-0.73	-0.85	6
	0.84	0.73	0.61	0.49	0.37	0.25	0.12	0.00	-0.12	-0.25	-0.37	-0.49	-0.61	-0.73	-0.84	9
	0.84	0.72	0.60	0.48	0.36	0.24	0.12	0.00	-0.12	-0.24	-0.36	-0.48	-0.60	-0.72	-0.84	12
	0.83	0.71	0.60	0.48	0.36	0.24	0.12	0.00	-0.12	-0.24	-0.36	-0.48	-0.60	-0.71	-0.83	15
	0.81	0.70	0.59	0.47	0.35	0.24	0.12	0.00	-0.12	-0.24	-0.35	-0.47	-0.59	-0.70	-0.81	18
	0.80	0.69	0.58	0.46	0.35	0.23	0.12	0.00	-0.12	-0.23	-0.35	-0.46	-0.58	-0.69	-0.80	21

Figure 5. Rolling moment due to pitch/yaw command.

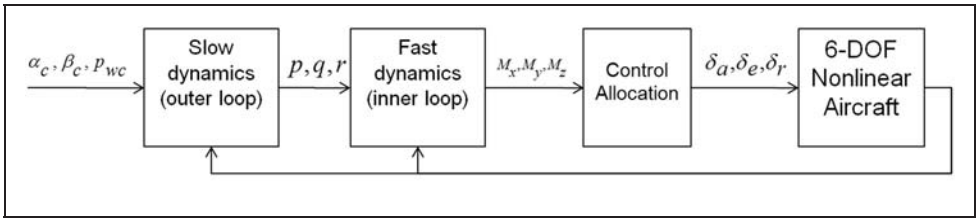

Figure 6. Airplane model with NDI controller.
NDI: nonlinear dynamic inversion.

force. The anti-symmetric deflection would generate both yawing and rolling moments as depicted in Figure 2(b).

Including the effect of the cant angle ϕ_N, forces and moments are modified as below.

Symmetric deflection:

$$\left.\begin{aligned} T_x &= 2T_G \cos\delta_N \\ T_y &= 0 \\ T_z &= -2T_G \sin\delta_N \cos\phi_N \end{aligned}\right\} \tag{9}$$

$$\left.\begin{aligned} M_x &= 0 \\ M_y &= 2T_G \cos\delta_G(Z_{CG} - Z_{CG}) \\ &\quad -2T_G \sin\delta_N \cos\phi_N(X_{CG} - X_{noz}) \\ M_z &= 0 \end{aligned}\right\} \tag{10}$$

Anti-symmetric deflection:

$$\left.\begin{aligned} T_x &= 2T_G \cos\delta_N \\ T_y &= 2T_G \sin\delta_N \sin\phi_N \\ T_z &= 0 \end{aligned}\right\} \tag{11}$$

$$\left.\begin{aligned} M_x &= -2T_G \sin\delta_N \cos\phi_N Y_{eng} \\ &\quad -2T_G \sin\delta_N \sin\phi_N(Z_{eng} - Z_{CG}) \\ M_y &= 2T_G \cos\delta_N(Z_{eng} - Z_{CG}) \\ M_z &= -2T_G \sin\delta_N \sin\phi_N(X_{CG} - X_{noz}) \end{aligned}\right\} \tag{12}$$

Independent left/right nozzle deflection:

$$\left.\begin{aligned} T_x &= T_{G,r}\cos\delta_{N,r} + T_{G,l}\cos\delta_{N,l} \\ T_y &= T_{G,r}\sin\delta_{N,r}\sin\phi_N - T_{G,l}\sin\delta_{N,l}\sin\phi_N \\ T_z &= -T_{G,r}\sin\delta_{N,r}\cos\phi_N - T_{G,l}\sin\delta_{N,l}\cos\phi_N \end{aligned}\right\} \tag{13}$$

$$\left.\begin{aligned} M_x &= (-T_{G,r}\sin\delta_{N,r} + T_{G,l}\sin\delta_{N,l})\cos\phi_N Y_{eng} \\ &\quad -(T_{G,r}\sin\delta_{N,r} - T_{G,l}\sin\delta_{N,l})\sin\phi_N(Z_{eng} - Z_{CG}) \\ M_y &= (T_{G,r}\cos\delta_{N,r} + T_{G,l}\cos\delta_{N,l})(Z_{eng} - Z_{CG}) \\ &\quad -(T_{G,r}\sin\delta_{N,r} + T_{G,l}\sin\delta_{N,l})\cos\phi_N(X_{CG} - X_{noz}) \\ M_z &= -(T_{G,r}\sin\delta_{N,r} - T_{G,l}\sin\delta_{N,l})\sin\phi_N(X_{CG} - X_{noz}) \\ &\quad +(-T_{G,r}\cos\delta_{N,r} + T_{G,l}\cos\delta_{N,l})Y_{eng} \end{aligned}\right\} \tag{14}$$

Equivalent left/right nozzle deflection

Single-axis vectoring with canted nozzles on twin-engine airplane can generate pitch and yaw moment as shown above. However, the left and right nozzles require to be controlled independently to generate the required pitch/yaw moments. The left/right nozzle commands equivalent to a pitch/yaw deflection command can be derived as follows.

Table 1. Level flight trims as initial conditions.

Altitude (m)	0	0	1000
Mach number	0.2	0.6	0.21
Speed (*V*) (m/s)	67.1	204	70.3
AOA (°)	20.0	2.126	20.0
Elevator (°)	−4.74	0.246	−4.81
Throttle (°)	38.9	36.6	39.8

The normal force and side force for a given pitch and yaw deflection of a multi-axis vector nozzle (from equation(1)) is

$$\left.\begin{aligned} T_y &= T_G \cos\,\delta_{ptv} \sin\,\delta_{ytv} \\ T_z &= -T_G \sin\,\delta_{ptv} \cos\,\delta_{ytv} \end{aligned}\right\} \tag{15}$$

which can be equated to the normal force and side force generated in single-axis canted nozzles (from equation (13))

$$\left.\begin{aligned} T_y &= T_G \sin\,\delta_r \sin\,\phi_N - T_G \sin\,\delta_l \sin\,\phi_N \\ T_z &= -T_G \sin\,\delta_r \cos\,\phi_N - T_G \sin\,\delta_l \cos\,\phi_N \end{aligned}\right\} \tag{16}$$

From equations (15) and (16)

$$\left.\begin{aligned} T_G \sin\,\phi_N(\sin\,\delta_r - \sin\,\delta_l) &= T_G \cos\,\delta_{ptv} \sin\,\delta_{ytv} \\ -T_G \cos\,\phi_N(\sin\,\delta_r + \sin\,\delta_l) &= -T_G \sin\,\delta_{ptv} \cos\,\delta_{ytv} \end{aligned}\right\} \tag{17}$$

From equation (17), one can arrive at the following equality relations:

$$\left.\begin{aligned} \sin\,\delta_r &= \frac{\sin\,\delta_{ptv} \cos\,\delta_{ytv}}{2\cos\,\phi_N} + \frac{\cos\,\delta_{ptv} \sin\,\delta_{ytv}}{2\sin\,\phi_N} \\ \sin\,\delta_l &= \frac{\sin\,\delta_{ptv} \cos\,\delta_{ytv}}{2\cos\,\phi_N} - \frac{\cos\,\delta_{ptv} \sin\,\delta_{ytv}}{2\sin\,\phi_N} \end{aligned}\right\} \tag{18}$$

Figures 3 and 4 show pitch and yaw control authority for the cant angle of 20° and 40°, respectively as obtained from equation (18).

The shaded region shows the achievable pitch and yaw commands limiting the nozzle deflection to 21°. As seen in Figure 3, the yaw control power is limited to 6° only, whereas the pitch control power available is up to 18°. When a combination of pitch and yaw control power is required, the control power available is further reduced. With 20° inclination of vector plane, available yaw control power is very small. Figure 4 shows the control power for 40° inclination angle of the vector plane. Here, the maximum authority is 15° in pitch and 12° in yaw. Hence, depending on the requirement of TVC power to augment the aerodynamic controls, an appropriate nozzle cant angle can be chosen during the design. It is to be noted that the single-axis vectoring with canted nozzles highly restrict the control authority as compared to multi-axis thrust vectoring though it offers simplicity in the vectoring mechanism. The other disadvantage of this nozzle mechanism is that it is not possible to produce pure yawing moment. The asymmetric deflection of the nozzle required to produce yawing moment also produces the rolling moment. From equation (14), the rolling moment per unit thrust neglecting the engine offset with CG in vertical plane is

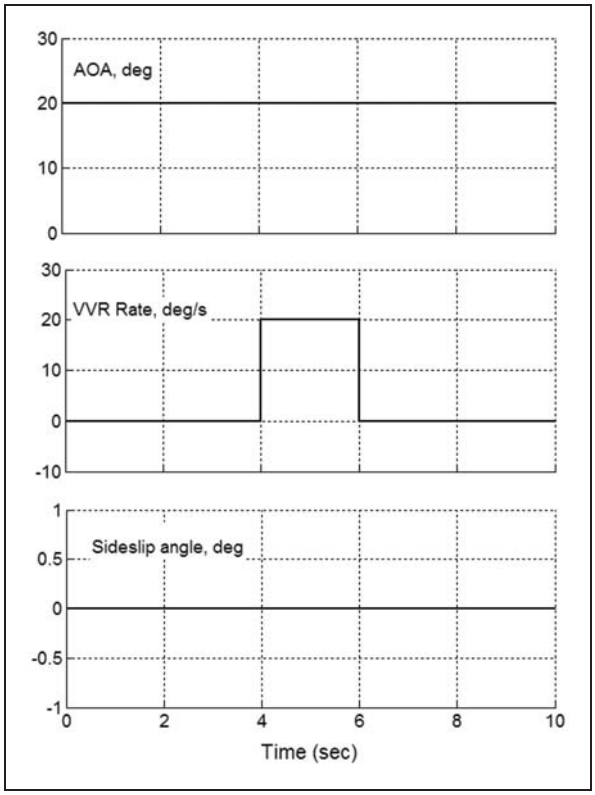

Figure 7. Command input for VVR simulation.
VVR: velocity vector roll.

$$M_x/T_G = \cos\,\phi_N(Y_{eng} - Y_{CG})(\sin\,\delta_{N,l} - \sin\,\delta_{N,r}) \tag{19}$$

The rolling moment produced per kilonewton of engine thrust for the pitch/yaw command with 2-m engine spacing and nozzle cant angle of 40° computed from equation (19) is shown in Figure 5. As seen from Figure 5, the pitch command does not produce the rolling moment, but the yaw command produces considerable yawing moment as the commanded yaw deflection increases. The design should ensure that the aileron has sufficient control power to counter this rolling moment. A positive yaw command produces negative yawing moment as discussed earlier. It also produces a negative rolling moment in this case. In other words, a negative roll command produces a negative yawing moment and hence it can be treated as *pro* yaw.

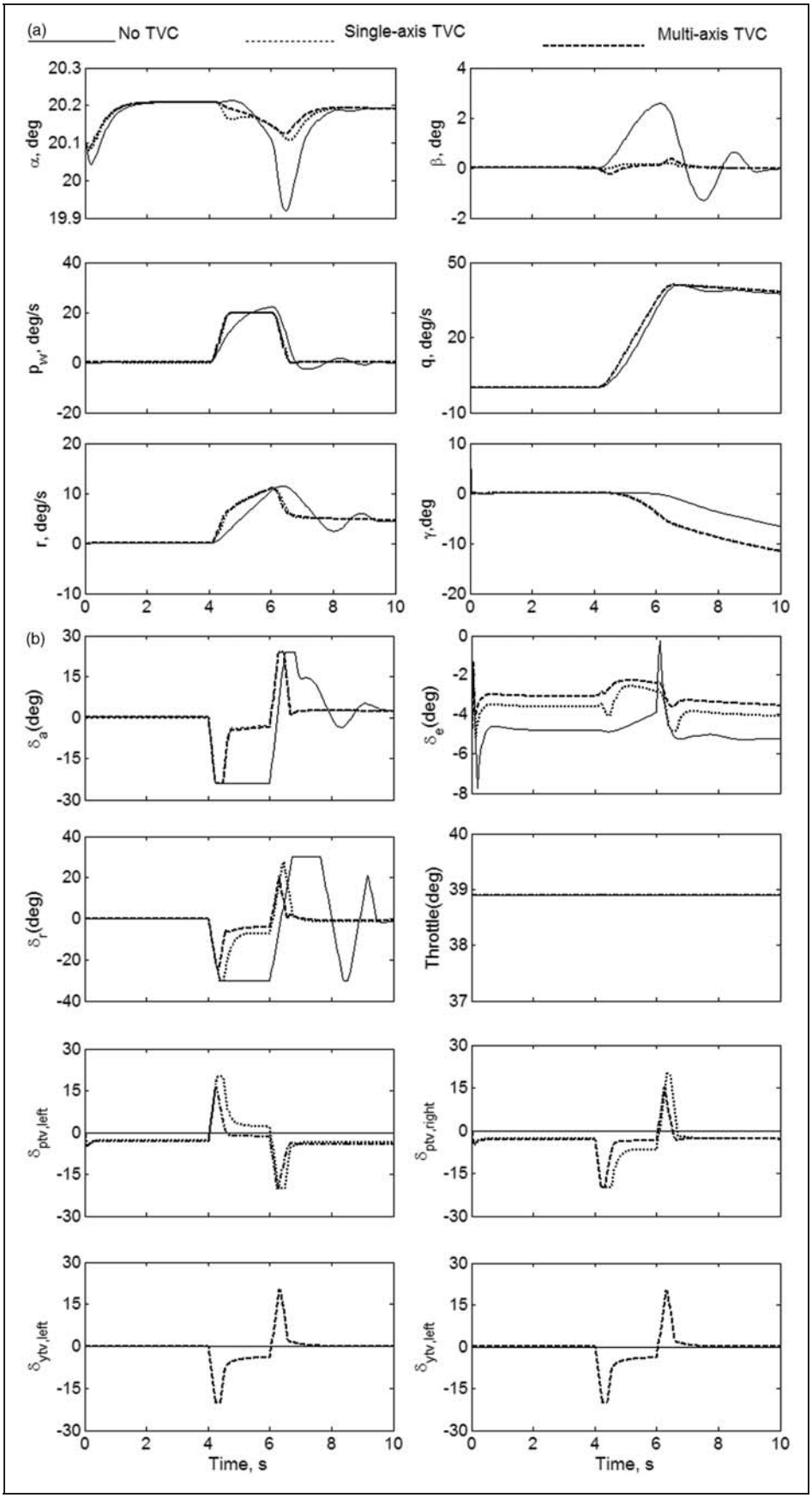

Figure 8. (a) Simulation time history – states and (b) Simulation time history – controls.

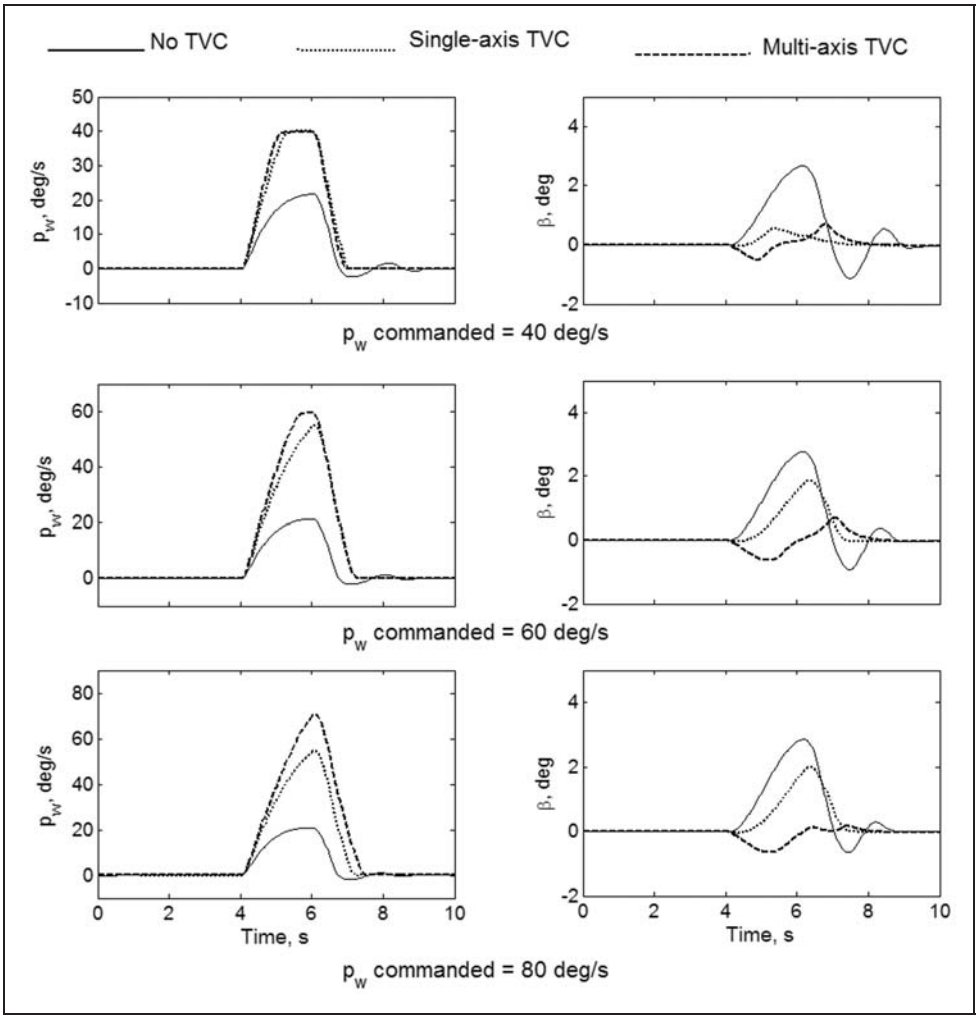

Figure 9. Results for different VVR commands.
VVR: velocity vector roll.

VVR Simulation with NDI control

NDI control is widely used in fast prototyping of control laws while evaluating different concepts. Hence, it is an ideal tool to be used for evaluating the different thrust vector concepts through 6-dof simulation. NDI controller finds the control schedule by inverting the dynamic equations. This methodology is very useful to quickly design a simple controller to evaluate alternate design options of a system. A dynamic system can be modeled as $f(x, \dot{x}, u) = 0$, which can be rewritten as

$$\dot{x} = f(x, u) \tag{20}$$

The NDI requires that the control terms are separated from the equations and are linear in control

$$\dot{x} = f(x) + g(x)u \tag{21}$$

Now, the control law can be written as

$$u = g^{-1}(x)[\dot{x} - f(x)] \tag{22}$$

The NDI as applied to airplane control requires that the airplane equations of motion are separated into fast dynamic states p, q, r and slow dynamic states α, β, ϕ.[10] This is necessary because the airplane has fewer control effectors than the states/outputs to be controlled. The control effectors control the fast dynamic states p, q, r in the inner loop and p, q, r control the slow states α, β, ϕ in the outer loop. The schematic of NDI control structure as applied to airplane is shown in Figure 6.

The F-18/HARV airplane was modeled in MatLab/Simulink. The F-18/HARV aerodata available from the NASA website[11] was used to make the flight dynamic model. The nonlinear model with NDI controller was developed and tested extensively for various maneuvers before using it for the present work. The control allocation was developed as a separate block which allocates the moments M_x, M_y and M_z to the available controls. This helps in implementing different control allocation methods when redundant controls such as thrust vector nozzles are available in addition to aerodynamic controls.

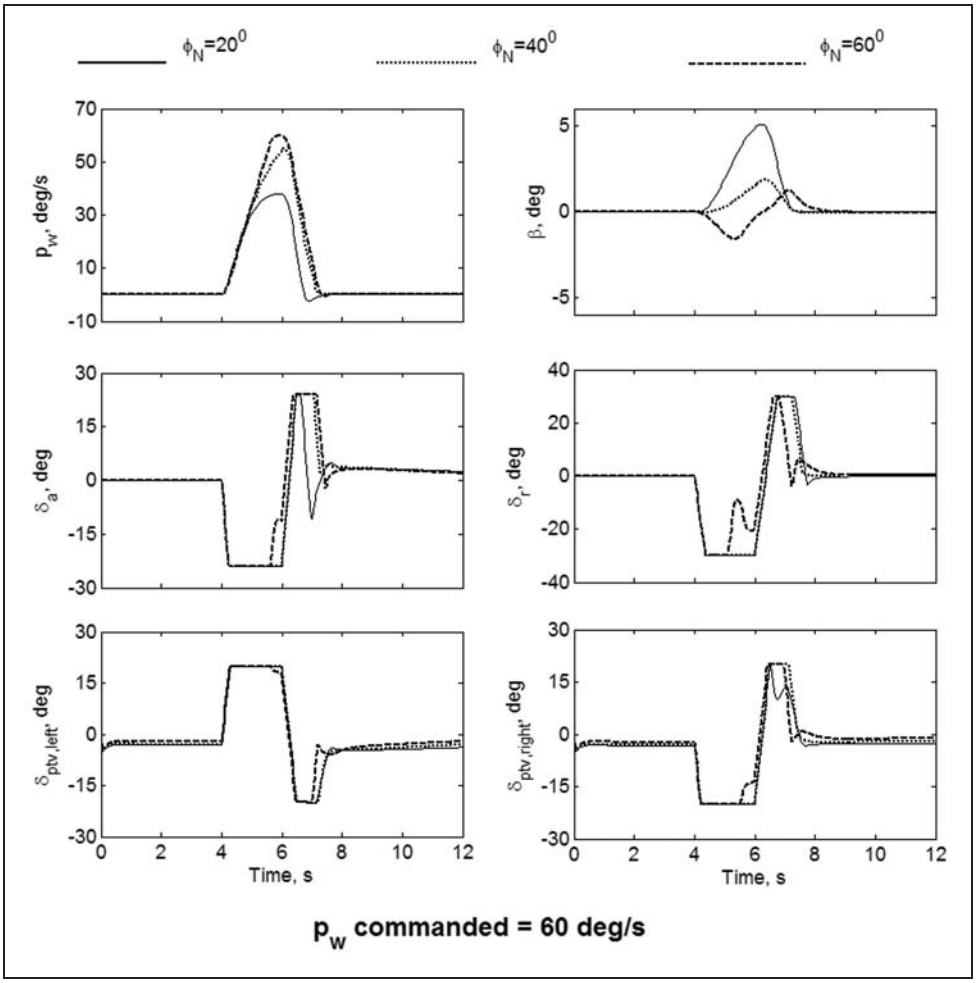

Figure 10. Results for VVR command of 4 s pulse.
VVR: velocity vector roll.

The roll rate in the wind axis system, i.e. the VVR rate is given by[12]

$$p_w = p\cos\alpha\cos\beta + (q-\dot{\alpha})\sin\beta + r\sin\alpha\cos\beta \tag{23}$$

The simulation of VVR is carried out by commanding wind axis (velocity vector) roll rate (p_w), AOA and angle of sideslip. The sideslip is commanded to zero and the AOA is corresponding to the 1-g trim. In the NDI slow dynamics loop, these commands are transformed into the body-axis angular rates p, q, r by inverting equation (24).

$$\begin{bmatrix} \cos\alpha\cos\beta & \sin\beta & \sin\alpha\cos\beta \\ -\cos\alpha\tan\beta & 1 & \sin\alpha\tan\beta \\ \sin\alpha & 0 & \cos\alpha \end{bmatrix} \begin{pmatrix} p \\ q \\ r \end{pmatrix} = \begin{bmatrix} p_w \\ (\alpha_c-\alpha)k_\alpha - \dfrac{1}{mV\cos\beta}[T_z + C_L\bar{q}S - mg\cos\mu\cos\gamma] \\ (\beta_c-\beta)k_\beta - \dfrac{1}{mV}[T_y + C_y\bar{q}S + mg\sin\mu\cos\gamma] \end{bmatrix} \tag{24}$$

The 6-dof rigid airplane equations of motion used for modeling[10,12] are given in Appendix 2.

Simulation results

The primary objective of this study is to evaluate the merits of different thrust vector nozzle concepts with respect to the VVR performance of an airplane. The simulation studies have been carried out starting from trimmed level flight conditions. Various simulations were performed at different initial flight conditions as given in Table 1.

Low speed VVR

The low speed VVR was carried out with simulations starting from trimmed 1-g flight condition with Mach 0.2 shown in Table 1. The VVR command in the form of a 2.0 s pulse was applied while commanding AOA at trim value and sideslip angle to zero as shown in Figure 7. The throttle was kept constant at the trim value.

The simulation results at 0.2 Mach with a commanded VVR rate of 20° are shown in Figure 8(a)

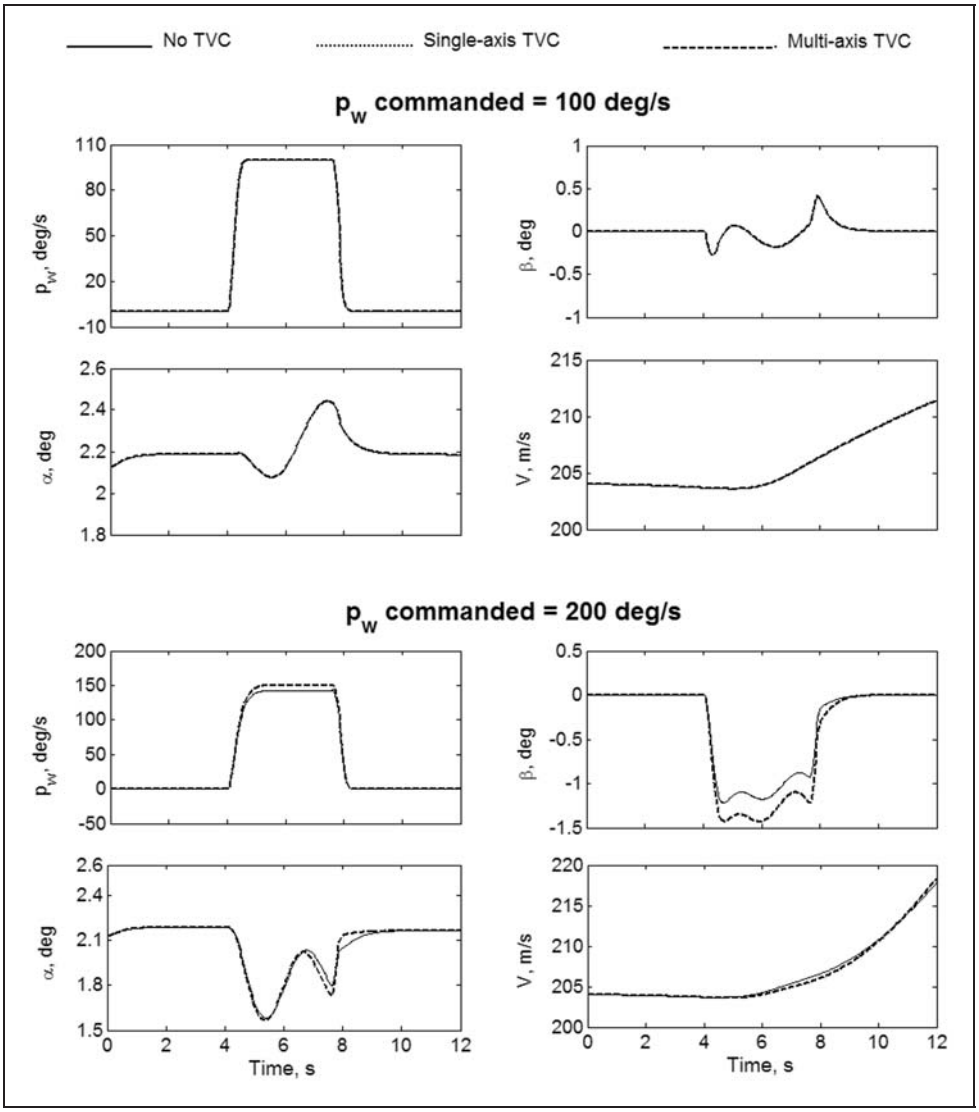

Figure 11. Results for VVR at Mach number $M = 0.6$.
VVR: velocity vector roll.

and (b). The simulation results with three different control schemes are compared in Figure 8(a) and (b). The first scheme uses only aerodynamic controls; the second uses single-axis vectoring with 40° canted nozzles and the third uses multi-axis TVC. As seen from the figure, the commanded VVR rate could be achieved in all three cases. However, the sideslip angle could not be controlled in the case where only aerodynamic controls were used. The maximum sideslip angle is 2.6° in the case of aerodynamic controls only and negligible in the other two cases. The reason for the buildup of sideslip is the saturation of rudder control as shown in Figure 8(b). In the case of TVC, there is no saturation of rudder as well as the vector nozzle, whereas with no TVC, the rudder saturates for a longer duration. The AOA deviation from the commanded value is negligible in all the three cases as the stabilator deflection required is well within the maximum limit. The airplane starts to descend (γ is negative) as the vertical component of lift decrease during the roll.

The analysis of control history is as follows. The aileron deflection is negative in order to command positive roll and is reversed after 2 s to stop the roll. The airplane also yaws to the right (positive r). There is adverse yaw due to the roll making the airplane sideslip to the left resulting in positive sideslip. The rudder acts to nullify the sideslip through negative deflection. When multi-axis TVC is used, both left and right nozzle yaw deflections are to the right in order to control the sideslip (in the same sense as rudder), and the pitch deflections are opposite (left nozzle down and right nozzle up) to augment the aileron for rolling to the right. However, when single-axis TVC is used, the left nozzle is deflected downward and right nozzle upward to generate positive yaw for controlling the positive sideslip. The stabilator schedule is different in all the three cases even in level flight (simulation

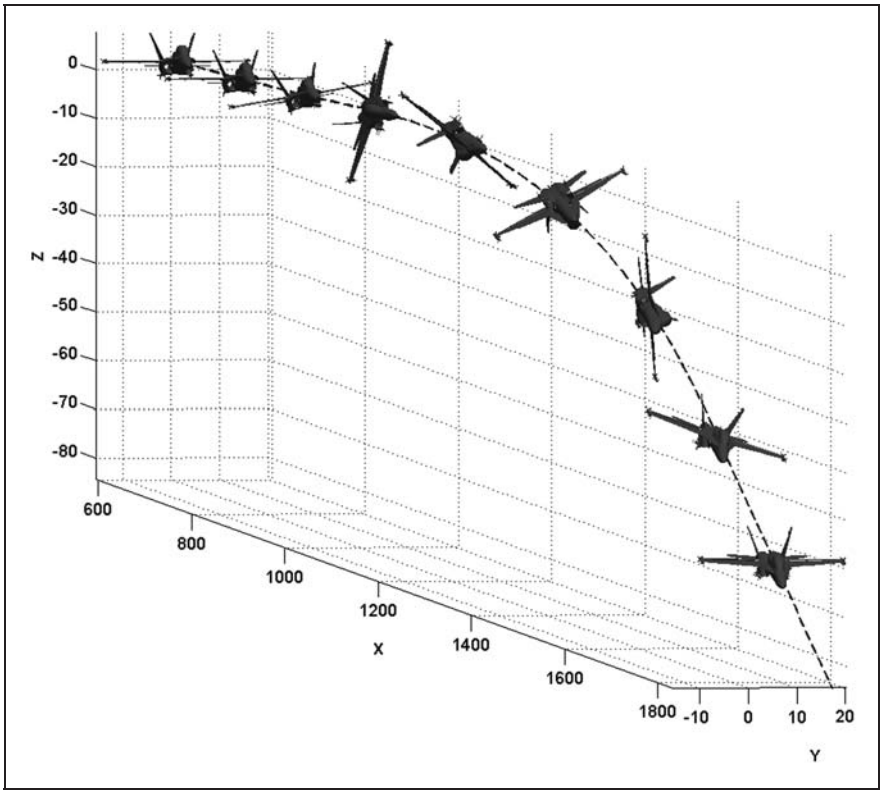

Figure 12. Pictorial representation of 360° VVR at Mach number $M = 0.6$.
VVR: velocity vector roll.

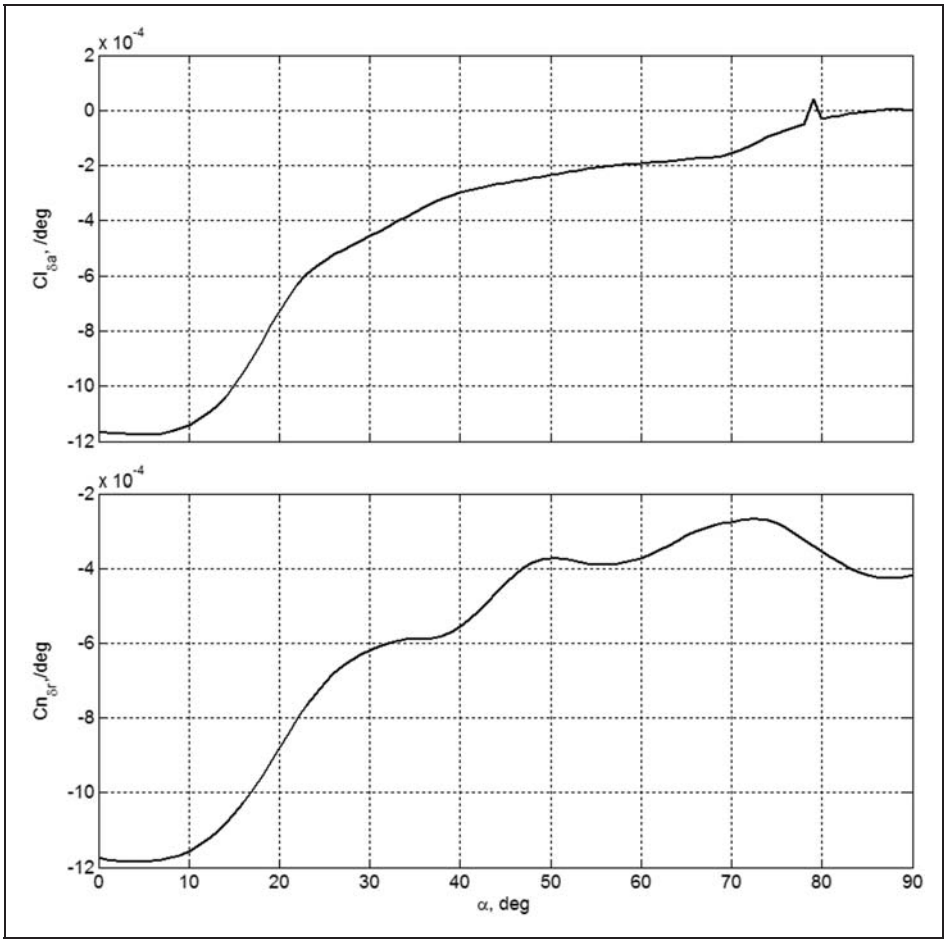

Figure 13. Aileron/Rudder control derivatives.

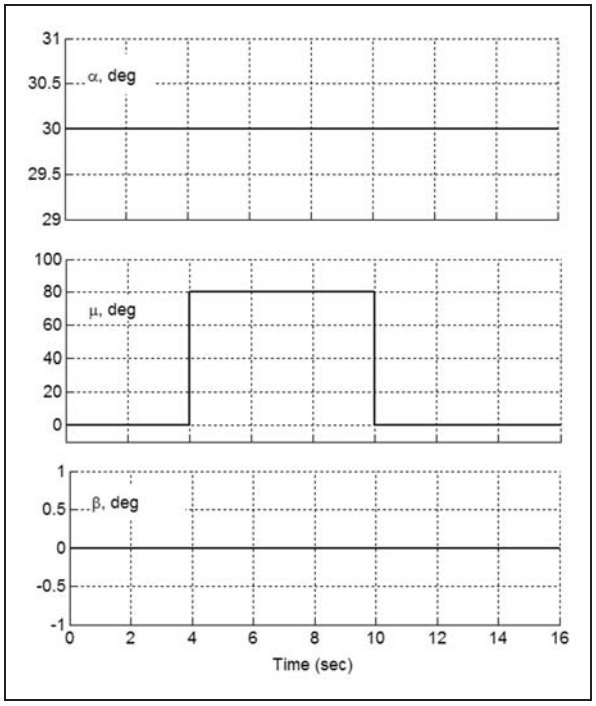

Figure 14. VVR command input.
VVR: velocity vector roll.

time before 4 s). The elevator is at -5° when TVC is not used, but when TVC is used, the total pitching moment to be produced is shared by both the pitch control effectors. The pseudo-inverse algorithm used for allocating the control moment among all the available control effectors minimizes the control effort.

Figure 9 shows the results of the simulation for higher VVR rate commands at the same speed of Mach 0.2 and AOA of 20°. As seen from the figure, VVR rate $>20^\circ$/s is not achievable without the use of TVC. The single-axis TVC is capable of achieving a roll rate of 40°/s without significant sideslip buildup, whereas the multi-axis TVC is capable of executing a roll rate of 60°/s. The roll rate buildup (i.e. slope of p_w curve or roll acceleration) is proportional to the roll control power, which increases from the case of only aerodynamic control to single-axis TVC and to multi-axis TVC. It is important to note that the sideslip is not increasing beyond 3°, which is because the VVR rate commanded had a pulse of 2 s duration only. In the case of $p_w = 80^\circ$/s command, the sideslip did not build up when multi-axis TVC was used, which indicates that there was no persistent saturation of rudder or the yaw vector control, but only requires more time to reach the commanded roll rate.

Effect of nozzle cant angle

In the single-axis TVC, the plane of vectoring can be chosen in the design. The cant angle (ϕ_N) of the nozzle (plane of vectoring) is a trade-off between the pitch and yaw control power requirement as discussed in section 'Thrust vector models'. From the VVR maneuver analyzed, it is evident that the requirement is for the higher yaw and roll control power and not for the pitch control power at 20° AOA. The elevator deflection required during the VVR was found to be well within the limits. The sensitivity of vectoring plane angle on the VVR maneuver was studied by setting the angle to 20°, 40° and 60°. The VVR rate commanded was 60°/s as shown in Figure 10. The increase in ϕ_N increases the yaw control power and helps in achieving higher VVR rate with good control on sideslip as shown in the figure.

High speed VRR

The VVR simulation at Mach 0.6, sea-level condition was carried out with two different rates 100°/s and 200°/s as shown in Figure 11. The high-speed VVR has been carried out to see if thrust vector can augment the aerodynamic control to improve the roll rate.

The results for 100°/s roll rate command show that all the three control types result in same response. This was expected because the aerodynamic controls are much more powerful than the TVC at high speed due to high dynamic pressure. For the commanded roll rate of 200°/s, the achieved roll rate is only about 150°/s with aerodynamic controls only and a little higher rate was obtained with the use of TVC. This was found to be due to insufficient roll control power of the ailerons which has saturated. The improvement in roll rate with TVC was only marginal because of the low engine power (throttle = 36.6). However, by using full reheat power of the engine (throttle = 100), it was possible to enhance the roll rate to 200°/s. The pictorial representation of the VVR simulation for 360° deg roll at the rate of 100°/s is shown in Figure 12. The loss in altitude and a small change in flight path angle can be seen in the figure.

High AOA VVR

A fighter airplane's VVR capability degrades quickly as the AOA increases. This is because of the reduction of control effectiveness of the aerodynamics controls (Figure 13) and also the reduction of dynamic pressure because of the low speed. The thrust vector nozzle enables VVR capability in low speed and high AOA regime.

In order to analyze the performance of different thrust vector nozzle concepts, simulation studies were carried out at 20.1° AOA, 0.2 Mach, sea-level conditions. The parametric studies carried out included the single-/multi-axis thrust vectoring and engine throttle setting. The inputs commanded for the simulation are shown in Figure 14. The initial condition is the trimmed level flight at Mach 0.2, at sea level. Throttle was set to the maximum afterburner thrust (throttle = 100°). A bank angle of 80°

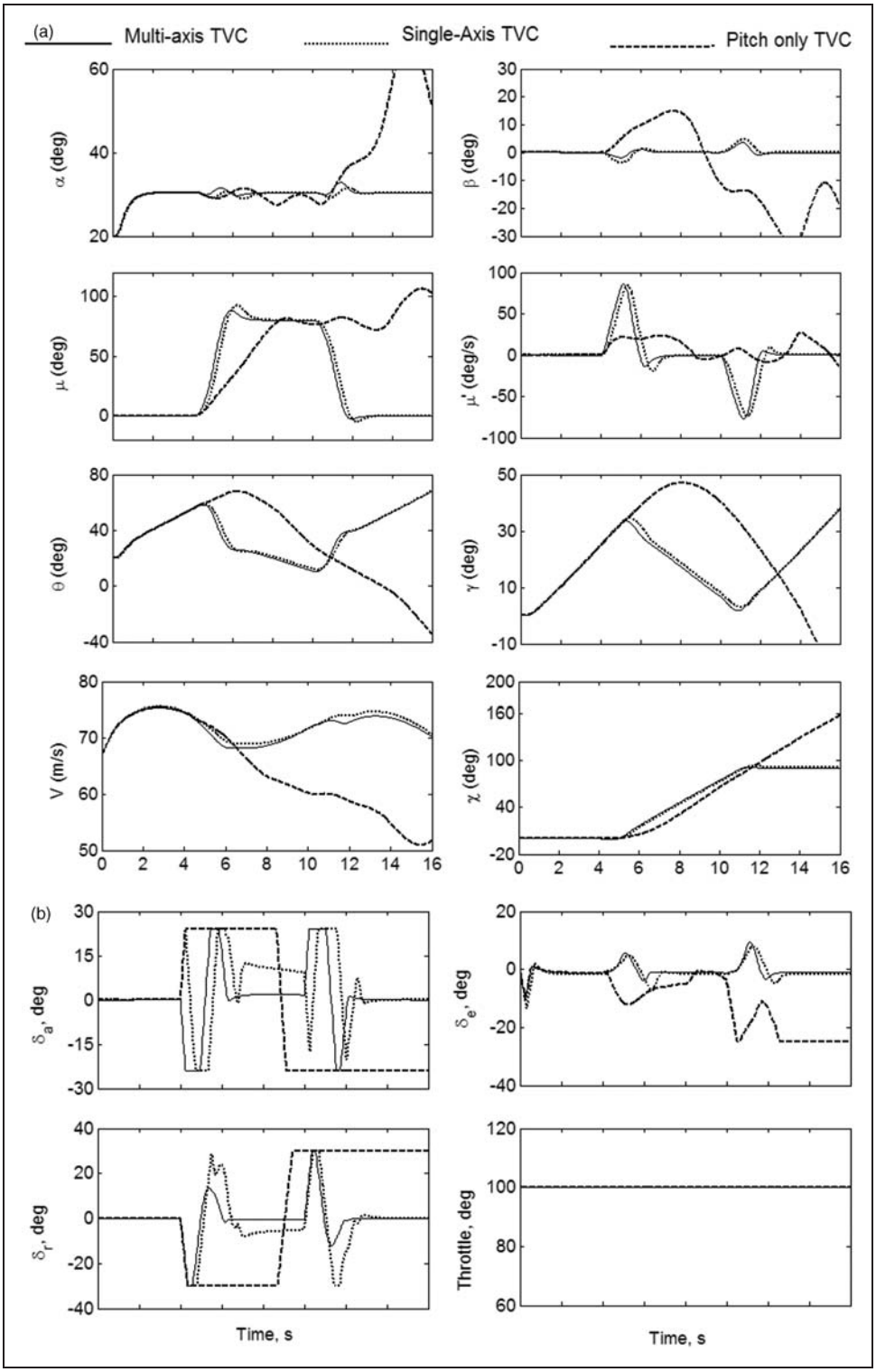

Figure 15. (a) High AOA VVR – states history and (b) high AOA VVR – multi-axis TVC.
AOA: angle of attack; VVR: velocity vector roll; TVC: thrust vector control.

was commended for 6 s duration. The AOA commanded was 30° throughout the maneuver and the sideslip was commanded to zero.

The simulation results with the multi-axis TVC, single-axis TVC with canted nozzles and pitch only TVC are shown in Figure 15. The commanded bank angle of 80° has reached in about 2 s for the case of multi-axis and single-axis canted nozzles TVC, whereas for the pitch only TVC it took about 4 s. In the case of pitch only TVC, the airplane did not respond to the roll back command to wings level attitude and the airplane departed to very high AOA with

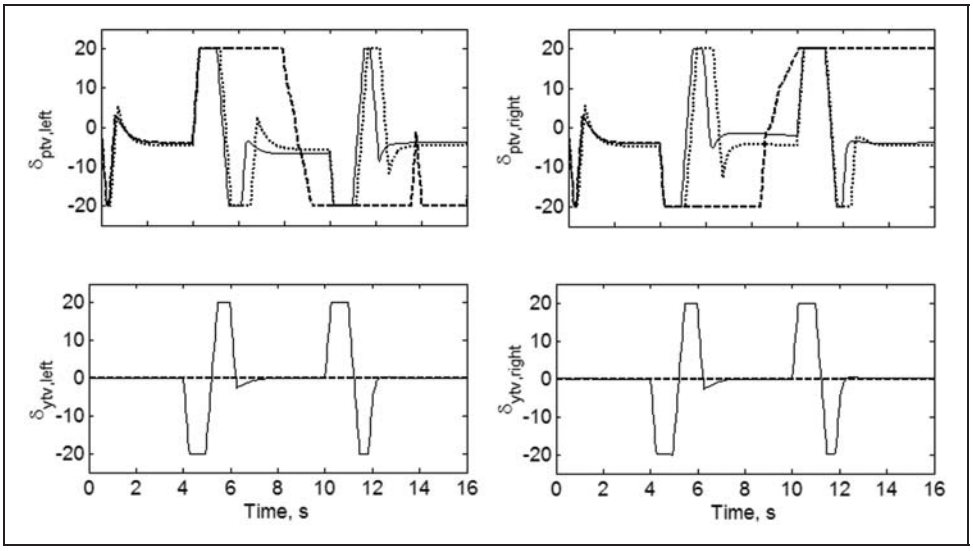

Figure 15. Continued.

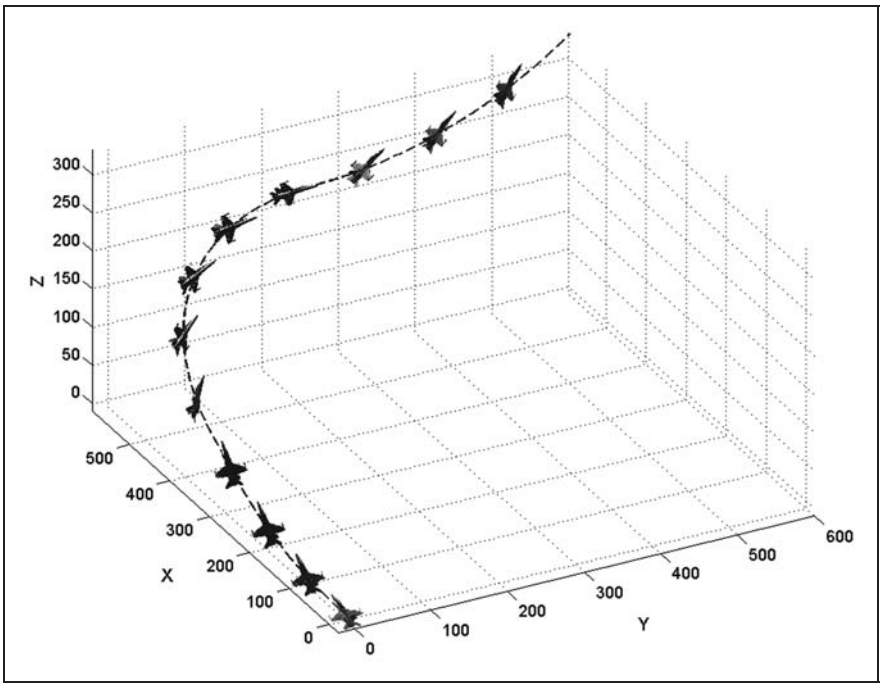

Figure 16. Pictorial view of high AOA VVR.
AOA: angle of attack; VVR: velocity vector roll.

large sideslip. The deviation in AOA and sideslip is negligible with the multi-axis and single-axis canted nozzles TVC. The maximum roll rate reached was 80°/s. The airplane climbs initially due to higher AOA commanded and due to full afterburner thrust and the climb angle reduces during the banked flight duration. The banked flight resulted in a heading change of about 90°.

The initial pitch up of the airplane from the trim AOA of 20.1° to the commanded AOA of 30° was executed with the left/right nozzles vectoring upward and also the stabilator deflection upward. The airplane roll to the right is executed by the negative deflection of the aileron and the differential deflection of the nozzles in pitch. The left nozzle is deflected downward and the right nozzle is deflected upward to generate positive rolling moment. The positive roll rate causes negative yawing moment and this is countered by negative deflection of both the rudder and yaw vector nozzles.

In the case of single-axis canted nozzles TVC, the rudder and the differential nozzles deflection is similar

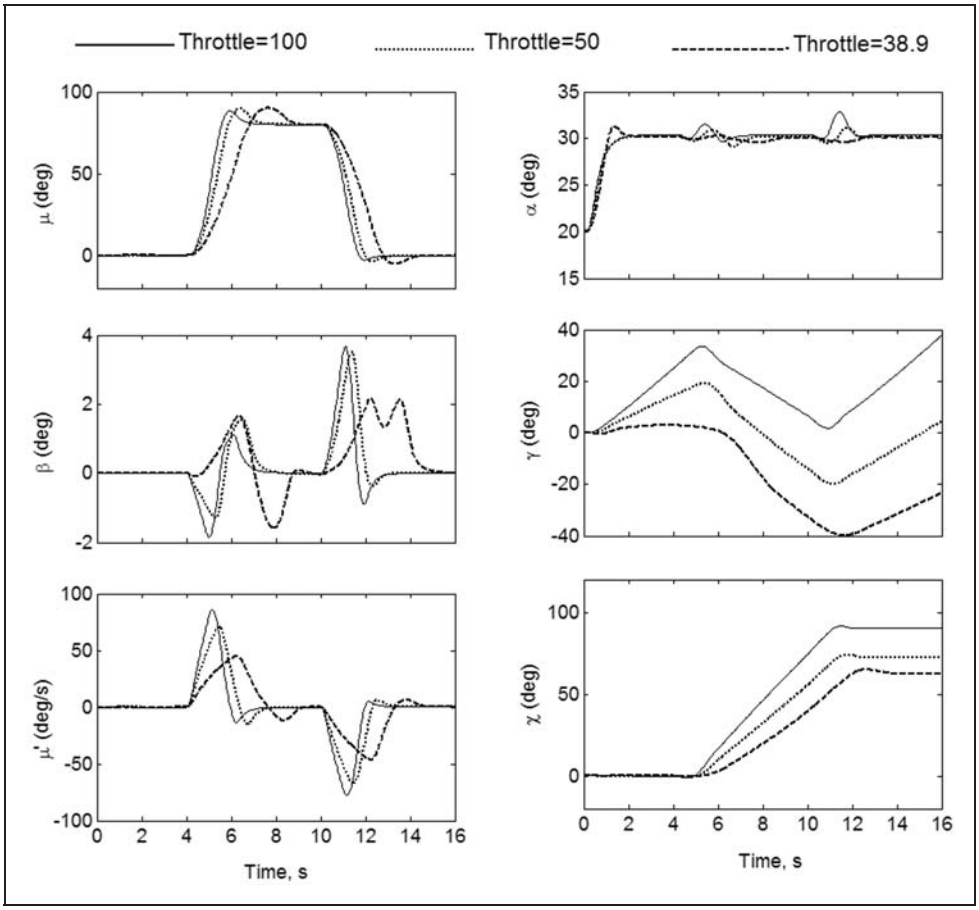

Figure 17. Effect of throttle on VVR.
VVR: velocity vector roll.

to the case of multi-axis vectoring. However, there is a marked difference in the aileron control. In the case of multi-axis TVC, the aileron deflection is negative to cause the positive roll as expected. In the case of single-axis TVC, the aileron is positive initially which is counter intuitive. This is because of the coupling between the yaw and roll control power of the single-axis vectoring with canted nozzles as discussed in section 'Thrust vector models'. The differential nozzle deflection generates both yaw and roll control power, and the rolling moment in this case exceeded the requirement and hence the aileron deflect in the opposite sense to reduce the rolling moment. A similar aileron deflection can be seen at $t = 10$ s when the airplane is commanded to roll back to wings level attitude.

In the case of pitch only TVC, the nozzles deflect differentially similar to other two cases, but unable to control the sideslip without the yaw control power from the vector nozzles. Even the AOA diverges due to lack of pitch control power, because the differential nozzle deflection continues to control the sideslip.

The pictorial view of the airplane 3-D trajectory with attitude is shown in Figure 16. The airplane heading has changed by about 90° and it continues to climb due to full afterburner power setting.

Effect of thrust in high AOA roll

The effect of thrust on the capability of VVR with TVC was studied by varying the engine throttle setting for a given VVR rate command. The throttle was set at 38.9 (trim), 50 (maximum dry) and 100 (maximum reheat) setting. The results are shown in Figure 17.

The TVC power at level flight throttle setting corresponding to $M = 0.2$ is low. There is an AOA overshoot and slower roll rate buildup at throttle = 38.9 as shown. However, the sideslip deviation is not large due to low roll rate. The flight path angle is reduced as the throttle is reduced. The heading change during the maneuver increases with the throttle setting. This could be contributed to the thrust effect on the flight path angle rather than the TVC power. The high throttle setting helps in steeper climb initially with thrust balancing significant part of airplane weight due to high pitch attitude. The same is also responsible for steeper descent when the pitch attitude is negative (Figure 15(a)).

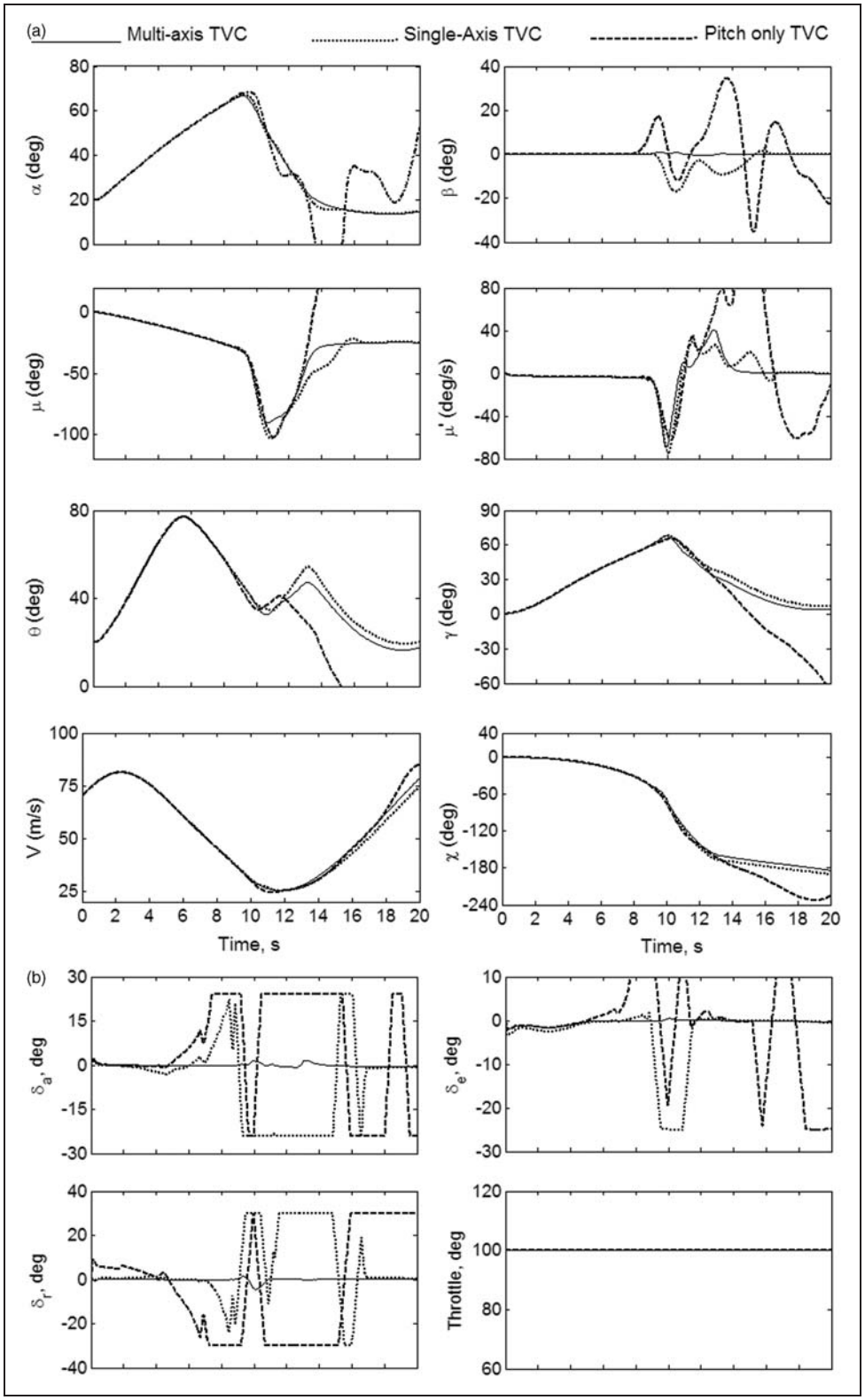

Figure 18. (a) Herbst maneuver: simulated time history of airplane state variables and (b) Herbst maneuver: simulated time history of airplane control variables.

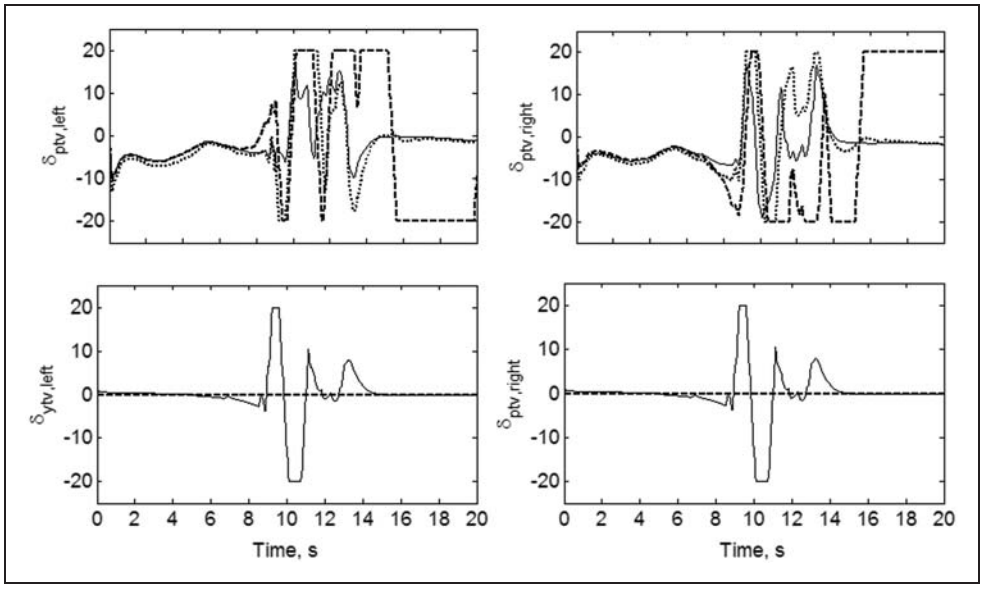

Figure 18. Continued.

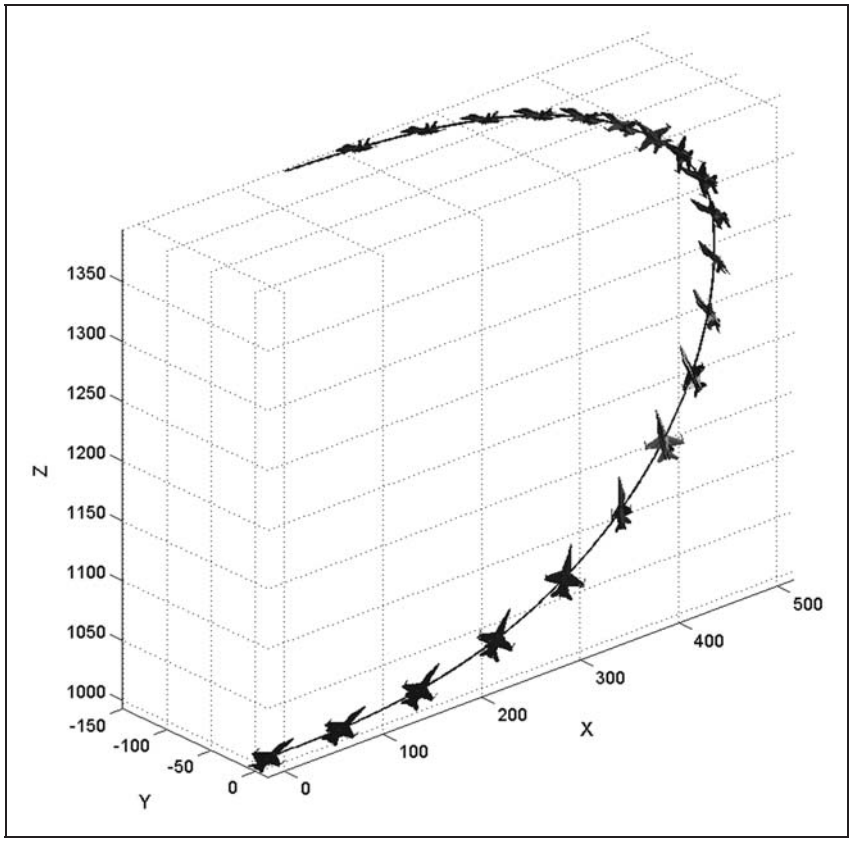

Figure 19. Pictorial view – Herbst maneuver.

Herbst maneuver

High AOA VVR is an important maneuver for a supermaneuverable airplane such as F-18/HARV. The Herbst maneuver named after Dr Herbst enables an airplane to quickly reverse its direction using a combination of high AOA and VVR. At the start of the maneuver, the airplane pitches up to high AOA and climbs while losing speed. At the top of the climb it rolls about the velocity vector to change the heading and dives to regain the lost speed. The maneuver was simulated using the optimum AOA and bank angle

command proposed in ref.[13] A tracking control for Herbst maneuver has been developed for F18/HARV airplane with multi-axis TVC without considering the roll control power from vector nozzles in this reference.

The simulation results of the Herbst maneuver is shown in Figure 18. The simulation has been carried out with multi-axis TVC, single-axis TVC with canted nozzles and pitch only TVC. The tracking of the commanded AOA and bank angle is fairly good using the multi-axis TVC. Previous study[13] shows poor tracking with ailerons constrained to $\pm 24^\circ$. However, the poor tracking could be contributed to the TVC not being used for the roll control in their model. The 3-D pictorial view of the maneuver is shown in Figure 19.

The results also show a not so good tracking of the controller with single-axis canted nozzles. Though the AOA tracking is good, the bank angle command tracking is poor, especially while pulling out of the bank. The VVR arrest was found to be more difficult than roll initiation as pointed out in ref.[14] There is also unacceptable sideslip generated due to the saturation of rudder and the vector nozzles. However, the flight path variable γ and χ closely matches with that of control with multi-axis TVC. In the case of pitch only TVC, the commands could not be tracked and the flight path departs completely from the commanded.

The control histories provide greater insight into the maneuver. In the case of multi-axis TVC, the aerodynamic controls are barely used because of the large control power available in pitch, roll and yaw from the thrust vector nozzles. The bank to the left is affected by the differential deflection of nozzles in pitch and asymmetric left/right nozzle yaw deflection controls the sideslip. In the case of the single-axis TVC, both roll control and yaw control have to be performed by the differential deflection of the vector nozzles. The pitch control is also affected by the vector nozzles initially, but when the roll activity peaks up, the pitch control is handed over to the stabilator as shown in the figure. The aileron deflection is counter intuitive (roll right moment) between $t = 10$ s and 15 s due to the coupling of roll/yaw control power of the single-axis vectoring with canted nozzles.

Conclusions

i. The thrust vector nozzle concepts such as multi-axis vectoring, pitch only thrust vector and single-axis vectoring with canted nozzles have been discussed along with the model equations for forces and moments. The limitations of single-axis canted nozzles were shown in terms of available yaw/pitch control power and the rolling moment and yawing moment coupling.
ii. The VVR has been simulated using NDI controller for the twin-engine airplane F18 HARV. At moderate speed of Mach 0.6, the thrust vector has little or no benefit in enhancing VVR rate as the TVC power is relatively small as compared with aerodynamic controls.
iii. At low speed and high AOA, the multi-axis thrust vector nozzle plays a crucial role in executing VVR. The single-axis thrust vectoring with canted nozzles is a compromise which enables moderate VVR maneuvers at low speed and high AOA. The limitations of single-axis canted nozzles TVC are twofold; the availability of lower control power in pitch and yaw as compared to multi-axis TVC and the coupling between the roll and yaw control power.
iv. The nozzle cant angle of single-axis canted nozzles should be at least about 40° to have significant yaw control authority to execute VVR at high AOA.
v. The pitch only thrust vector nozzle is a special case of the single-axis canted nozzles where the cant angle (ϕ_N) is zero. The pitch vector nozzle on twin-engine airplane can provide pitch and roll control power. The pitch and roll control are not coupled, i.e. the pitch and roll moments can be commanded independent of each other within the available limits.
vi. The engine thrust effect on high AOA VVR is very significant both in enhancing TVC power and reducing the airplane descent rate for sufficiently longer duration.
vii. The multi-axis TVC and single-axis canted nozzles TVC are effective in tracking the Herbst maneuver command, whereas the pitch only TVC is unable to execute the maneuver.

Funding

This research received no specific grant from any funding agency in the public, commercial, or not-for-profit sectors.

Conflict of interest

None declared.

References

1. Capone FJ and Mason ML. Multi-axis aircraft control power from thrust vectoring at high angles of attack. NASA-TM-87741, 1986.
2. O'Rourke MJ, Ralston JN, Bell JW, et al. PC-based simulation of the F-16/MATV. In: *AIAA modeling and simulation technologies conference*, New Orleans, LA, 11–13 August 1997, AIAA-3728.
3. Barham RW. Thrust vector aided maneuvering of the YF-22 advanced tactical fighter prototype. In: *AGARD meeting on technologies for highly maneuverable aircraft*, Annapolis, MD, USA, 18–21 October 1993.
4. Atesoglu O and Ozgoren MK. Velocity vector roll control of a fighter aircraft with multi-axis thrust vector control. In: *IFAC workshop on aerospace guidance. Navigation and flight control systems*, Samara, Russia, 30 June–2 July 2009.

5. Alcorn CW, Croom MA, Francis, et al. The X-31 aircraft advances in aircraft agility and performance. *Prog Aerosp Sci* 1996; 32(4): 377–413.
6. Sinha NK and Ananthkrishnan N. Bifurcation analysis of inertia coupled roll maneuvers of airplanes. *Proc IMechE, Part G: J Aerospace Engineering* 2003; 217: 75–85.
7. Goman MG, Khramtsovsky AV and Kolesnikov EN. Investigation of the ADMIRE maneuvering capabilities using qualitative methods, nonlinear analysis and synthesis techniques for aircraft control. *Lect Notes Control Inf Sci* 2007; 365: 301–324.
8. Scalera KR. *A Comparison of control allocation methods for the F-15 ACTIVE research aircraft utilizing real-time piloted simulations*. MS Thesis, Aerospace Engineering, Virginia Polytechnic Institute, 1999.
9. Bundick WT, Pahle JW and Yeager JC. Design of a mixer for the thrust-vectoring system on the high-alpha research vehicle. NASA-TM-110228, 1996.
10. Snell SA, Enns DF and Garrard WL. Nonlinear inversion flight control for a supermaneuverable aircraft. *J Guid Control Dyn* 1992; 15(4): 976–984.
11. Dunbar B. *Documentation for a Dynamic Inversion Control Law Proposed for RFCS, Dryden Flight Research Center*, http://www.nasa.gov/centers/dryden/history/pastprojects/HARV/Work/NASA2/nasa2.html (2008).
12. Durham B. Equations of motion, Chapter 7, http://www.dept.aoe.vt.edu/~durham/AOE5214/Ch07.pdf.
13. Pourtakdoust SH, Karimi J and Shajiee S. Design of a tracking control system for an optimal post-stall manoeuvre using dynamic inversion approach. In: *25th International congress of the aeronautical sciences*, Hamburg, Germany, 3–8 September 2006.
14. Boyum KE, Pachter M and Houpis CM. High angle of attack velocity vector rolls. *Control Eng Pract* 1995; 3(8): 1087–1093.

Appendix 1

Notation

D	drag
F	force
L	lift
m	airplane mass
m_0	engine air flow rate
M_x, M_y, M_z	rolling, pitching and yawing moments, respectively
p, q, r	body-axis roll, pitch and yaw rates, respectively
T	thrust
V	velocity
α	angle of attack
β	angle of sideslip
δ	control deflection
μ, γ, χ	flight path orientation angles (bank, climb, heading)
ϕ_N	nozzle vector plane inclination
ϕ, θ, ψ	Euler angles (roll/pitch/yaw)

Subscripts.

a, e, r	aileron/stabilator/rudder
c	commanded
eng	engine
G	gross
l, r	left/right
N, noz	nozzle
ptv, ytv	pitch/yaw thrust vector
w	wind axis
x, y, z	body-axis components
0, IN	inlet

Appendix 2

Rigid airplane equations of motion (12 states)

$$\dot{V} = \frac{1}{m}[-D\cos\beta + (F_y + T_y)\sin\beta + T_x\cos\alpha\cos\beta + T_z\sin\alpha\cos\beta + mg(-\cos\alpha\cos\beta\sin\theta + \sin\beta\cos\theta\sin\phi + \sin\alpha\cos\beta\cos\theta\cos\phi)]$$

$$\dot{\alpha} = q - \tan\beta(p\cos\alpha + r\sin\alpha) + \frac{1}{mV\cos\beta}[-L + T_z\cos\alpha - T_x\sin\alpha + mg(\cos\alpha\cos\theta\cos\phi + \sin\alpha\sin\theta)]$$

$$\dot{\beta} = (p\sin\alpha - r\cos\alpha) + \frac{1}{mV}[(F_y + T_y)\cos\beta + D\sin\beta - T_x\cos\alpha\sin\beta - T_z\sin\alpha\sin\beta + mg(\cos\alpha\sin\beta\sin\theta + \cos\beta\cos\theta\sin\phi - \sin\alpha\sin\beta\cos\theta\cos\phi)]$$

$$\dot{p} = qr(I_y - I_z)/I_x + \frac{1}{2I_x}\rho V^2 SbC_l(\alpha, \beta, \delta_a, \delta_e, \delta_r)$$

$$\dot{q} = rp(I_z - I_x)/I_y + \frac{1}{2I_y}\rho V^2 ScC_m(\alpha, \beta, \delta_a, \delta_e, \delta_r)$$

$$\dot{r} = pq(I_x - I_y)/I_z + \frac{1}{2I_z}\rho V^2 SbC_n(\alpha, \beta, \delta_a, \delta_e, \delta_r)$$

$$\dot{\chi} = p + q\sin\phi\tan\theta + r\cos\phi\tan\theta$$

$$\dot{\theta} = q\cos\phi - r\sin\phi$$

$$\dot{\psi} = q\sin\phi\sec\theta + r\cos\phi\sec\theta$$

$$\dot{x} = u\cos\psi\cos\theta + v(-\sin\psi\cos\phi + \cos\psi\sin\theta\sin\phi) + w(\sin\psi\sin\phi + \cos\psi\sin\theta\cos\phi)$$

$$\dot{y} = u\sin\psi\cos\theta + v(\cos\psi\cos\phi + \sin\psi\sin\theta\sin\phi) + w(-\cos\psi\sin\phi + \sin\psi\sin\theta\cos\phi)$$

$$\dot{z} = -u\sin\theta + v\cos\theta\sin\phi + w\cos\theta\cos\phi$$

Additional equations for navigational states

$$\dot{\mu} = \sec\beta(p\cos\alpha + r\sin\alpha) - \frac{g}{V}\cos\gamma\cos\mu\tan\beta + \frac{L}{mV}(\tan\gamma\sin\mu + \tan\beta) + \frac{(F_y + T_y)}{mV}\tan\gamma\cos\mu\cos\beta + \frac{1}{mV}(T_x\sin\alpha - T_z\cos\alpha)(\tan\gamma\sin\mu + \tan\beta) - \frac{1}{mV}(T_x\cos\alpha + T_z\sin\alpha)\tan\gamma\cos\mu\sin\beta$$

$$\dot{\gamma} = \frac{1}{mV}\{L\cos\mu - mg\cos\gamma - (F_y + T_y)\sin\mu\cos\beta\} + \frac{T_x}{mV}\{\sin\mu\sin\beta\cos\alpha + \cos\mu\sin\alpha\} + \frac{T_z}{mV}\{\sin\mu\sin\beta\sin\alpha - \cos\mu\cos\alpha\}$$

$$\dot{\chi} = \frac{1}{mV\cos\gamma}\{L\sin\mu + (F_y + T_y)\cos\mu\cos\beta + T_x(\sin\mu\sin\alpha - \cos\mu\sin\beta\cos\alpha)\} - \frac{T_z}{mV\cos\gamma}\{\cos\mu\sin\beta\sin\alpha + \sin\mu\cos\alpha\}$$